A TANH Spline Interpolation Technique for Modelling Ion Channels: Application to BK Channels in Smooth Muscle

Suranjana Gupta
Department of Biosciences and Bioengineering
IIT Bombay, Powai 400076
Mumbai, India
suranjana.gupta@ieee.org

Rohit Manchanda
Department of Biosciences and Bioengineering
IIT Bombay, Powai 400076
Mumbai, India
rmanch@iitb.ac.in

***Abstract*—Ion channels are molecular entities that are responsible for electrical signal generation in nerve, muscle and other cells. The paper discusses the use of hyperbolic tangent functions (TANH) in the modelling of the Big Conductance Potassium (BK) ion channel, especially for the smooth muscle of the urinary bladder. Ion channels are often modelled using the Hodgkin-Huxley formalism, in which equations governing the dependencies of various state parameters on cellular variables are derived from experimental data. When there is sufficient experimental data, formulating equations that replicate the trend becomes relatively easy. However, where the data for these dependencies is sparse, usual approaches fail. Formerly, we had described a TANH spline interpolation technique as an efficient means of fitting sparse data [1]. Here, we show that this technique also accurately predicts the actual trend via the interpolation. Furthermore, this spline interpolation technique could be extended in cases where there exist sufficient data points but no definite trend can be ascertained. TANH is used to "braid" functions in two or more adjacent regions and is done, unlike with splines, in a way such that a single function operates over the whole region. The resultant function is whole range, continuous and differentiable to any arbitrary order. We have demonstrated the application of this technique in modelling the parameter "slope factor" for the BK channel of mammalian smooth muscle. We show that, by the use of this technique, BK channel current outputs thus generated, faithfully replicate physiologically recorded BK currents from the detrusor smooth muscles of guinea-pig bladder. We propose this method as one that can be applied to modelling ion channels that are either characterized by sparse data, or that possess abundant but scattered experimental data.**

Keywords-Interpolation, Hyperbolic tangent, Slope factor, BK ion channel, Smooth muscle, Urinary bladder

I. INTRODUCTION

Ion channels are amongst the most important and crucial parts of any tissue. The variants help in controlling and modulating the excitability of the cell. These play a role in the rising and falling phases of the action potential, or "spike", which is an active signal central to coding and propagation of excitation in nerve and muscle cells. These channels are targets for most pharmacological drugs. By understanding the nature of their functional role in the respective tissues, drug designers can manufacture highly potent and efficacious drugs.

The BK channels, amongst the other known channels, have the highest single channel conductance of (100 – 300) pS [2]. These channels activate with the rise in intracellular calcium concentration and membrane voltage [3]. These play a very dominant role in controlling the repolarization phase of the action potential [4] as well as the resting membrane potential [5]. In the bladder, these maintain the tone and excitability of the smooth muscle and regulate spontaneous phasic contractions [6].

Absence or mutations in the channel contribute to overactive bladders as well as neurogenic detrusor overactivity [7, 8]. For instance, BK channels are being used to treat overactive bladders [5, 8] either by administering BK channel openers or by injecting the BK gene into the cell.

The BK channel current comprises two components, the steady state BK current and the transient BK current (TBKC). Studies have been performed to characterize these components of currents with respect to the underlying sources of calcium concentration because these channels are powerfully driven by cytosolic calcium levels [3, 9].

In modelling ion channels, it becomes necessary to find the best-fit equations for parameters that are functions of voltage, calcium or other cellular variables. Various techniques have evolved to improve the ease of implementation. Lagrangian interpolation is used to fit N+1 data points to an N^{th} degree polynomial. Spline interpolation is a special technique used to "knot" together [10] piecewise functions. It accomplishes smoothness at the region boundaries by imposing conditions of continuity of the functions and a finite number of derivatives depending on the order of the function. An example of such a spline is the cubic-spline [11].

When there is sufficient experimental data, formulating equations that mimic the trend becomes relatively easy. However, the challenge arises when the data are sparse. It is difficult to infer the trend from sparse data. Any assumption made while approximating a sparse set of data points will invariably result in a certain level of bias. Thus, the resulting interpretation becomes a function of one's experience. Since the data is sparse, it may not be feasible to estimate a trend objectively. We have attempted to eliminate this element of

subjectivity by employing piecewise interpolation instead of approximation.

Another situation that could arise in which these existing interpolation and approximation techniques do not suffice is when there exist sufficient but scattered data points. In such a case, fitting a trend without user bias becomes challenging since no benefit can be derived from the ample data as it does not provide an insight into the underlying trend. We describe a new spline interpolation technique based on the hyperbolic tangent (TANH) function that can be used to overcome such difficulties.

The distinctive characteristic of the TANH function is used to stitch piecewise functions in two or more adjacent regions and is done in a way such that there is a single function valid over the whole region. The interpolation is constructed like a spline and is hence, created in parts. However, the resultant function is whole range and not piecewise. It is continuous and differentiable to any arbitrary order, as all of these parts are well stitched together to create an overall continuous function. In a way, it can be viewed as a spline that is "braided" instead of being "knotted".

II. Hyperbolic Tangent Spline Function

A. *Two-region Hyperbolic Tangent Interpolation*

Consider two polynomials $P_n(x)$ and $Q_m(x)$, of degrees n and m respectively. The data points over which these polynomials exist range from $x_0, x_1, x_2, ..., x_\gamma$, i.e., $\gamma+1$ data points (Figure 1). A single, whole range Lagrangian interpolation will result in a $(\gamma)^{th}$ degree polynomial.

$P_n(x)$ is constructed from $n+1$ data points, and $Q_m(x)$ is constructed from $\gamma-n$ data points.

$$P_n(x) \to x_0, x_1, x_2, ..., x_{n-1}, x_n$$

and

$$Q_m(x) \to x_{n+1}, x_{n+2}, ..., x_{\gamma-1}, x_\gamma$$

Here, the following must hold identically true:

$$n+m=\gamma-1 \tag{1}$$

The polynomials can be expressed as:

$$P_n(x) = p_0 + p_1x + p_2x^2 + ... + p_{n-1}x^{n-1} + p_nx^n \tag{2}$$

$$Q_m(x) = q_0 + q_1x + q_2x^2 + ... + q_{m-1}x^{m-1} + q_mx^m \tag{3}$$

Consider a point ξ_n that lies in between x_n and x_{n+1} such that

$$\xi_n \triangleq \frac{x_n + x_{n+1}}{2} \tag{4}$$

Here we propose that,

$$\begin{aligned} Y &= [P(x) * f(x)] + [Q(x) * g(x)] \\ &= [P_n(x) * 0.5 * (1 - \tanh(k * (x - \xi_n)))] + \\ &\quad [Q_m(x) * 0.5 * (1 + \tanh(k * (x - \xi_n)))] \end{aligned} \tag{5}$$

This can be re-written as:

$$\frac{Y}{0.5} = [P_n(x) + Q_m(x)] + \tanh(k(x-\xi_n)) * [Q_m(x) - P_n(x)] \tag{6}$$

From (5) and Figure 1, we can assess that when:

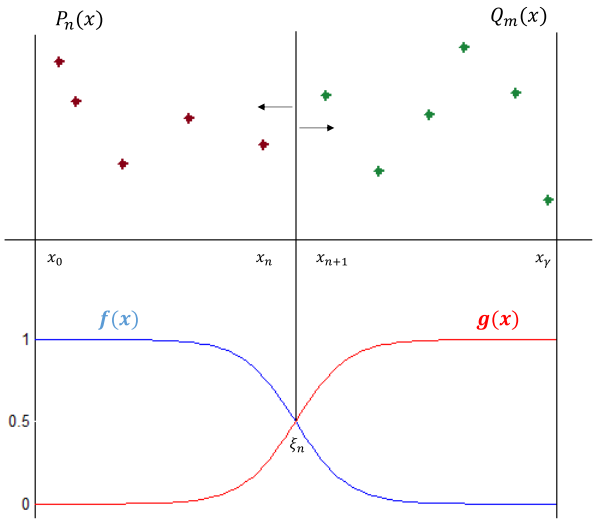

Figure 1. Graphical representation of the two-region TANH spline interpolation technique.

$$x \ll \xi_n \Rightarrow Y = P_n(x) \tag{7}$$

$$x \gg \xi_n \Rightarrow Y = Q_m(x) \tag{8}$$

However, around the point of transition ξ_n, the resulting function $Y(x)$ will comprise of both $P_n(x)$ and $Q_m(x)$. According to (7) and (8), a transition occurs from $P_n(x)$ to $Q_m(x)$ between x_n and x_{n+1}. The "rate" of this transition can be decided by k, which is also an unknown. k determines the steepness of fall of $f(x)$ and the rise of $g(x)$. It will effectively decide how many data points of $P_n(x)$ will modulate $Q_m(x)$ and vice-versa. Hence, k can be determined keeping in mind a certain range of permissible error.

Let the gaps between adjacent x_i be denoted by δ, i.e.,

$$\delta = x_{i+1} - x_i \tag{9}$$

then,

$$\xi_n = n\delta + \frac{\delta}{2} \tag{10}$$

At the transitional junction, one can deduce from (4) and (10):

$$(\xi_n - x_n) = (x_{n+1} - \xi_n) = \frac{\delta}{2} \tag{11}$$

Effectively, the splicing function takes the form of $\tanh(k * \delta/2)$ and based on the error margin, the value of k can be decided. For example: If the permissible error margin for this transition is $\pm 0.01\%$, then

$$\tanh(k * \delta/2) = 0.999 = \tanh(4)$$

$$\Rightarrow k = \frac{8}{\delta} \tag{12}$$

In order to ascertain the value of $P_n(x)$ and $Q_m(x)$, one must solve for the unknowns in (2) and (3).

1) Case 1: $m > n$ (13)

On substituting (2) and (3) into (6) and expanding the terms, we get the following expression:

$$\begin{aligned}&\frac{y_i}{0.5} = p_0 + p_1x_i + p_2{x_i}^2 + \ldots\ldots\ldots + p_{n-1}{x_i}^{n-1} + p_n{x_i}^n + \\ &q_0 + q_1x_i + q_2{x_i}^2 + \ldots\ldots\ldots + q_n{x_i}^n + \ldots\ldots\ldots + q_m{x_i}^m + \\ &[\tanh(k(x_i - \xi_n))*[q_0 + q_1x_i + \ldots + q_n{x_i}^n + \ldots + q_m{x_i}^m]] \\ &-[\tanh(k(x_i - \xi_n))*[p_0 + p_1x_i + \ldots\ldots\ldots + p_n{x_i}^n]]\end{aligned} \tag{14}$$

Let,

$$\tanh(k*(x_i - \xi_n)) = \eta_i \tag{15}$$

Substituting in (14) and combining the like terms,

$$\begin{aligned}&\frac{y_i}{0.5} = (p_0 + q_0) + (p_1 + q_1)x_i + \ldots\ldots + (p_n + q_n){x_i}^n \\ &+\eta_i(q_0 - p_0) + \eta_i(q_1 - p_1)x_i + \ldots\ldots + \eta_i(q_n - p_n){x_i}^n \\ &+(1+\eta_i)q_{n+1}{x_i}^{n+1} + \ldots\ldots\ldots + (1+\eta_i)q_m{x_i}^m\end{aligned} \tag{16}$$

This can be represented as follows in matrix notation:

$$\mathbf{Y = X * B} \tag{17}$$

where,

$$\mathbf{Y} = \begin{bmatrix} y_0/0.5 \\ y_1/0.5 \\ \vdots \\ y_\gamma/0.5 \end{bmatrix} \tag{18}$$

$$\mathbf{X} = \begin{bmatrix} 1 & x_0 & {x_0}^2 & \cdots & {x_0}^n & \eta_0 & \eta_0x_0 & \cdots & \eta_0{x_0}^n & (1+\eta_0){x_0}^{n+1} & \cdots & (1+\eta_0){x_0}^m \\ 1 & x_1 & {x_1}^2 & \cdots & {x_1}^n & \eta_1 & \eta_1x_1 & \cdots & \eta_1{x_1}^n & (1+\eta_1){x_1}^{n+1} & \cdots & (1+\eta_1){x_1}^m \\ \vdots & \vdots & \vdots & \ddots & \vdots & \vdots & \vdots & \ddots & \vdots & \vdots & \ddots & \vdots \\ 1 & x_\gamma & {x_\gamma}^2 & \cdots & {x_\gamma}^n & \eta_\gamma & \eta_\gamma x_\gamma & \cdots & \eta_\gamma{x_\gamma}^n & (1+\eta_\gamma){x_\gamma}^{n+1} & \cdots & (1+\eta_\gamma){x_\gamma}^m \end{bmatrix} \tag{19}$$

$$\mathbf{B} = \begin{bmatrix} p_0 + q_0 \\ p_1 + q_1 \\ p_2 + q_2 \\ \vdots \\ p_n + q_n \\ q_0 - p_0 \\ q_1 - p_1 \\ \vdots \\ q_n - p_n \\ q_{n+1} \\ \vdots \\ q_m \end{bmatrix} \tag{20}$$

The solution is thus:

$$\mathbf{B = X^{-1} * Y} \tag{21}$$

Once **B** is solved, its coefficients can be substituted in (16) to obtain the resulting interpolated function.

2) Case 2: $n > m$ (22)

The overall interpolated function is given by:

$$\begin{aligned}&\frac{y_i}{0.5} = p_0 + p_1x_i + p_2{x_i}^2 + \ldots\ldots\ldots + p_m{x_i}^m + \ldots. + p_n{x_i}^n \\ &+q_0 + q_1x_i + q_2{x_i}^2 + \ldots\ldots\ldots + q_m{x_i}^m \\ &+[\tanh(k(x_i - \xi_n))*[q_0 + q_1x_i + q_2{x_i}^2 + \ldots. + q_m{x_i}^m \\ &-p_0 - p_1x_i - p_2{x_i}^2 - \ldots\ldots - p_m{x_i}^m - \ldots\ldots - p_n{x_i}^n]]\end{aligned} \tag{23}$$

On substituting (15),

$$\begin{aligned}&\frac{y_i}{0.5} = (p_0 + q_0) + (p_1 + q_1)x_i + \ldots\ldots + (p_m + q_m){x_i}^m \\ &+\eta_i(q_0 - p_0) + \eta_i(q_1 - p_1)x_i + \ldots\ldots + \eta_i(q_m - p_m){x_i}^m \\ &+(1-\eta_i)p_{m+1}{x_i}^{m+1} + \ldots\ldots\ldots + (1-\eta_i)p_n{x_i}^n\end{aligned} \tag{24}$$

This can be represented in matrix notation as shown in (17). The matrix **Y** has exactly the same form as in (18) whereas, **X** and **B** take the following forms:

$$\mathbf{X} = \begin{bmatrix} 1 & x_0 & {x_0}^2 & \cdots & {x_0}^m & \eta_0 & \eta_0x_0 & \cdots & \eta_0{x_0}^m & (1-\eta_0){x_0}^{m+1} & \cdots & (1-\eta_0){x_0}^n \\ 1 & x_1 & {x_1}^2 & \cdots & {x_1}^m & \eta_1 & \eta_1x_1 & \cdots & \eta_1{x_1}^m & (1-\eta_1){x_1}^{m+1} & \cdots & (1-\eta_1){x_1}^n \\ \vdots & \vdots & \vdots & \ddots & \vdots & \vdots & \vdots & \ddots & \vdots & \vdots & \ddots & \vdots \\ 1 & x_\gamma & {x_\gamma}^2 & \cdots & {x_\gamma}^m & \eta_\gamma & \eta_\gamma x_\gamma & \cdots & \eta_\gamma{x_\gamma}^m & (1-\eta_\gamma){x_\gamma}^{m+1} & \cdots & (1-\eta_\gamma){x_\gamma}^n \end{bmatrix} \tag{25}$$

$$\mathbf{B} = \begin{bmatrix} p_0 + q_0 \\ p_1 + q_1 \\ p_2 + q_2 \\ \vdots \\ p_m + q_m \\ q_0 - p_0 \\ q_1 - p_1 \\ \vdots \\ q_m - p_m \\ p_{m+1} \\ \vdots \\ p_n \end{bmatrix} \tag{26}$$

The coefficients of **B** can be obtained using (21). These coefficients of **B** can be substituted into (24) to obtain the final equation.

3) Case 3: $n = m$ (27)

The resulting equation would be of the following form:

$$\begin{aligned}&\frac{y_i}{0.5} = (p_0 + q_0) + (p_1 + q_1)x_i + \ldots\ldots + (p_n + q_n){x_i}^n \\ &+\eta_i(q_0 - p_0) + \eta_i(q_1 - p_1)x_i + \ldots\ldots + \eta_i(q_n - p_n){x_i}^n\end{aligned} \tag{28}$$

(28) can be expressed using the matrix notation, where the matrices **X** and **B** will be of the following forms:

$$\mathbf{X} = \begin{bmatrix} 1 & x_0 & {x_0}^2 & \cdots & {x_0}^n & \eta_0 & \eta_0x_0 & \eta_0{x_0}^2 & \cdots & \eta_0{x_0}^n \\ 1 & x_1 & {x_1}^2 & \cdots & {x_1}^n & \eta_1 & \eta_1x_1 & \eta_1{x_1}^2 & \cdots & \eta_1{x_1}^n \\ \vdots & \vdots & \vdots & \ddots & \vdots & \vdots & \vdots & \vdots & \ddots & \vdots \\ 1 & x_\gamma & {x_\gamma}^2 & \cdots & {x_\gamma}^n & \eta_\gamma & \eta_\gamma x_\gamma & \eta_\gamma{x_\gamma}^2 & \cdots & \eta_\gamma{x_\gamma}^n \end{bmatrix} \tag{29}$$

and,

$$\mathbf{B} = \begin{bmatrix} p_0 + q_0 \\ p_1 + q_1 \\ p_2 + q_2 \\ \vdots \\ p_n + q_n \\ q_0 - p_0 \\ q_1 - p_1 \\ q_2 - p_2 \\ \vdots \\ q_n - p_n \end{bmatrix} \tag{30}$$

These coefficients of **B** can be substituted in (28) to obtain the final overall interpolated function.

An example can be considered to illustrate the working of this technique. Consider a set of data points (red circles) as shown in Figure 2. This set of data points have been manually digitized from Figure 2E in Herzog *et al.* [12]. This is further elucidated in Section IV (see DISCUSSION).

One region of these data points can be approximated by a rising exponential function whereas, the adjacent region as a falling exponential function. The two exponential functions could be interpolated, using (5), to provide an accurate fit (blue solid line) to the experimental data.

The equations used are as follows:

$$f(v) = 0.5 - 0.5\tanh(k*(v-\xi)) \tag{31}$$

$$g(v) = 0.5 + 0.5\tanh(k*(v-\xi)) \tag{32}$$

Here, $\xi = -42mV$ and $k = 0.2$

$$P(v) = 0.30494 + 32.78375*\exp(0.04149*v) \tag{33}$$

$$Q(v) = 0.54766 + 1.20782*\exp(-v/24.71602) \tag{34}$$

It must be noted that k and ξ are degrees of freedom that the users can take advantage of. For instance, in Figure 2, if $k = 1$, the rounded peak would be replaced with a much sharper and pointed peak, depicting the steepness with which the overall function is transitioning from $P(v)$ to $Q(v)$.

B. Three-region Hyperbolic Tangent Interpolation

In the previous section, the interpolated function was derived by dividing the data points over two regions. Now, let another data distribution be added to the existing range of data. Let these additional data points be $x_{\gamma+1}, ..., x_{\Gamma}$. Therefore, the new data set after the inclusion of the additional data has $\Gamma + 1$ data points.

One can address this by choosing a method similar to the one discussed in Section II A. Here, instead of two regions, three regions are created. These can be treated as two macro-regions, where the first macro-region comprises of two micro-regions, with data points from $x_0, x_1, x_2, ..., x_\gamma$. This macro-region is spanned by $Y(x)$ which has been found by implementing the TANH interpolation technique on $P_n(x)$ and $Q_m(x)$. The second macro-region is spanned by

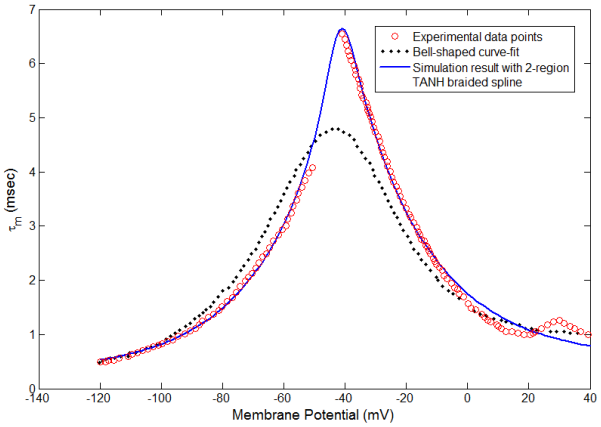

Figure 2. Proof of concept of implementation of two-region TANH interpolation technique, indicated in blue solid line. The red circles represent the experimental activation time constants for TTX-R persistent channels in spinal sensory neurons; the black dotted line depicts the bell-shaped curve that the authors had chosen to fit their experimental data. The latter two have been manually digitized from Figure 2E in Herzog *et al.* [12].

$Z_r(x)$, a polynomial of degree r, which is constructed from $\Gamma - \gamma$ data points i.e., $x_{\gamma+1}, ..., x_{\Gamma}$, (Figure 3). Here,

$$r = \Gamma - \gamma - 1 \tag{35}$$

and

$$Z_r(x) = z_0 + z_1 x + z_2 x^2 + ... + z_r x^r \tag{36}$$

These two macro-regions can now be interpolated using the TANH technique to produce a function that exists for the whole range of data (Figure 3).

Here, the overall whole-ranged function can be given by:

$$\frac{W}{0.5} = [Y(x) + Z_r(x)] + \tanh(K(x-\Xi))*[Z_r(x) - Y(x)] \tag{37}$$

Let,

$$\tanh(K*(x_i - \Xi)) = \mathrm{H}_i \tag{38}$$

On substituting (6), (15) and (38) in (37), we obtain:

$$\frac{W}{0.5} = \{[P(x) + Q(x)] + [\eta*[Q(x) - P(x)]] + Z(x)\} + \mathrm{H}*\{Z(x) - [[P(x) + Q(x)] + [\eta*[Q(x) - P(x)]]]\} \tag{39}$$

On further simplifying,

$$\frac{W}{0.5} = (P + Q + Z) + [\mathrm{H}*(Z - P - Q)] + [(1 - \mathrm{H})*\eta*(Q - P)] \tag{40}$$

Similar to the previous case, the rate of transition from $Y(x)$ to $Z(x)$ will be controlled by K, whereas the transition point is Ξ. Both these parameters provide extra degrees of freedom to the users.

1) Case 1: $n > m > r$ (41)

On substituting the expressions for $P(x)$, $Q(x)$ and $Z(x)$, given by (2), (3) and (36) respectively, in (40), the following is obtained:

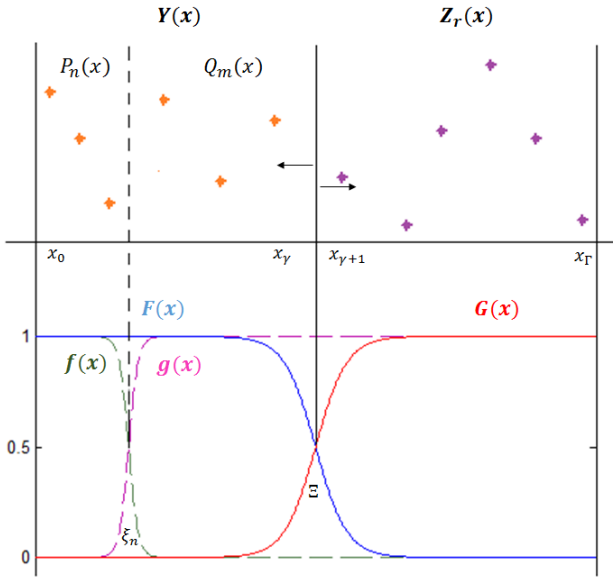

Figure 3. Graphical representation of the three-region TANH spline interpolation technique.

$$\frac{W}{0.5} = (p_0+q_0+z_0)+(p_1+q_1+z_1)x+....+(p_r+q_r+z_r)x^r$$
$$+\mathrm{H}(z_0-p_0-q_0)+\mathrm{H}(z_1-p_1-q_1)x+...+\mathrm{H}(z_r-p_r-q_r)x^r$$
$$+(1-\mathrm{H})(p_{r+1}+q_{r+1})x^{r+1}+.....+(1-\mathrm{H})(p_m+q_m)x^m$$
$$+(1-\mathrm{H})*\eta*(q_0-p_0)+.....+(1-\mathrm{H})*\eta*(q_m-p_m)x^m$$
$$+(1-\mathrm{H})*(1-\eta)*p_{m+1}x^{m+1}+....+(1-\mathrm{H})*(1-\eta)*p_nx^n \quad (42)$$

This can be expressed in matrix notation as:

$$\mathbf{W} = \mathbf{X}*\mathbf{D} \quad (43)$$

where,

$$\mathbf{W} = \begin{bmatrix} w_0/0.5 \\ \vdots \\ w_\gamma/0.5 \\ \vdots \\ w_\Gamma/0.5 \end{bmatrix} \quad (44)$$

$$\mathbf{X} = \begin{bmatrix} 1 & x_0 & \cdots & x_0^r & \mathrm{H}_0 & \mathrm{H}_0x_0 & \cdots & \mathrm{H}_0x_0^r & (1-\mathrm{H}_0)x_0^{r+1} & \cdots & (1-\mathrm{H}_0)x_0^m & \bullet \\ \vdots & \vdots & \ddots & \vdots & \vdots & \vdots & \ddots & \vdots & \vdots & \ddots & \vdots & \vdots \\ 1 & x_\gamma & \cdots & x_\gamma^r & \mathrm{H}_\gamma & \mathrm{H}_\gamma x_\gamma & \cdots & \mathrm{H}_\gamma x_\gamma^r & (1-\mathrm{H}_\gamma)x_\gamma^{r+1} & \cdots & (1-\mathrm{H}_\gamma)x_\gamma^m & \bullet \\ \vdots & \vdots & \ddots & \vdots & \vdots & \vdots & \ddots & \vdots & \vdots & \ddots & \vdots & \vdots \\ 1 & x_\Gamma & \cdots & x_\Gamma^r & \mathrm{H}_\Gamma & \mathrm{H}_\Gamma x_\Gamma & \cdots & \mathrm{H}_\Gamma x_\Gamma^r & (1-\mathrm{H}_\Gamma)x_\Gamma^{r+1} & \cdots & (1-\mathrm{H}_\Gamma)x_\Gamma^m & \bullet \\ \bullet & (1-\mathrm{H}_0)\eta_0 & \cdots & (1-\mathrm{H}_0)\eta_0x_0^m & (1-\mathrm{H}_0)(1-\eta_0)x_0^{m+1} & \cdots & (1-\mathrm{H}_0)(1-\eta_0)x_0^n \\ \vdots & \vdots & \ddots & \vdots & \vdots & \ddots & \vdots \\ \bullet & (1-\mathrm{H}_\gamma)\eta_\gamma & \cdots & (1-\mathrm{H}_\gamma)\eta_\gamma x_\gamma^m & (1-\mathrm{H}_\gamma)(1-\eta_\gamma)x_\gamma^{m+1} & \cdots & (1-\mathrm{H}_\gamma)(1-\eta_\gamma)x_\gamma^n \\ \vdots & \vdots & \ddots & \vdots & \vdots & \ddots & \vdots \\ \bullet & (1-\mathrm{H}_\Gamma)\eta_\Gamma & \cdots & (1-\mathrm{H}_\Gamma)\eta_\Gamma x_\Gamma^m & (1-\mathrm{H}_\Gamma)(1-\eta_\Gamma)x_\Gamma^{m+1} & \cdots & (1-\mathrm{H}_\Gamma)(1-\eta_\Gamma)x_\Gamma^n \end{bmatrix} \quad (45)$$

Here, $\bullet$ signifies continuation of the matrix.

$$\mathbf{D} = \begin{bmatrix} p_0+q_0+z_0 \\ p_1+q_1+z_1 \\ \vdots \\ p_r+q_r+z_r \\ z_0-p_0-q_0 \\ z_1-p_1-q_1 \\ \vdots \\ z_r-p_r-q_r \\ p_{r+1}+q_{r+1} \\ \vdots \\ p_m+q_m \\ q_0-p_0 \\ \vdots \\ q_m-p_m \\ p_{m+1} \\ \vdots \\ p_n \end{bmatrix} \quad (46)$$

The solution is:

$$\mathbf{D} = \mathbf{X}^{-1}*\mathbf{W} \quad (47)$$

On solving for $\mathbf{D}$, the coefficients can be substituted in (42) to obtain the overall function.

a) Case 1.1: $n = m > r$ (48)

This can be evaluated by simply substituting the equality $n = m$ in (45) and (46). In (42), all terms of the form $(1-\mathrm{H}_i)*(1-\eta_i)*p_jx_i^j$ will be eliminated.

b) Case 1.2: $n > m = r$ (49)

This can be evaluated by simply substituting the equality $r = m$ in (45) and (46). In (42), all terms of the form $(1-\mathrm{H}_i)(p_j+q_j)x_i^j$ will be eliminated.

2) Case 2: $m > n > r$ (50)

The overall function is given by:

$$\frac{W}{0.5} = (p_0+q_0+z_0)+(p_1+q_1+z_1)x+....+(p_r+q_r+z_r)x^r$$
$$+\mathrm{H}(z_0-p_0-q_0)+\mathrm{H}(z_1-p_1-q_1)x+...+\mathrm{H}(z_r-p_r-q_r)x^r$$
$$+(1-\mathrm{H})(p_{r+1}+q_{r+1})x^{r+1}+.....+(1-\mathrm{H})(p_n+q_n)x^n$$
$$+(1-\mathrm{H})*\eta*(q_0-p_0)+.....+(1-\mathrm{H})*\eta*(q_n-p_n)x^n$$
$$+(1-\mathrm{H})*(1+\eta)*q_{n+1}x^{n+1}+....+(1-\mathrm{H})*(1+\eta)*q_mx^m \quad (51)$$

This can be expressed using the matrix notation as provided in (43). $\mathbf{W}$ has the exact same form as shown in (44).

$$\mathbf{X}=\begin{bmatrix}
1 & x_0 & \cdots & x_0^{\,r} & \mathrm{H}_0 & \mathrm{H}_0x_0 & \cdots & \mathrm{H}_0x_0^{\,r} & (1-\mathrm{H}_0)x_0^{\,r+1} & \cdots & (1-\mathrm{H}_0)x_0^{\,n} & \bullet \\
\vdots & \vdots & \ddots & \vdots & \vdots & \vdots & \ddots & \vdots & \vdots & \ddots & \vdots & \vdots \\
1 & x_\gamma & \cdots & x_\gamma^{\,r} & \mathrm{H}_\gamma & \mathrm{H}_\gamma x_\gamma & \cdots & \mathrm{H}_\gamma x_\gamma^{\,r} & (1-\mathrm{H}_\gamma)x_\gamma^{\,r+1} & \cdots & (1-\mathrm{H}_\gamma)x_\gamma^{\,n} & \bullet \\
\vdots & \vdots & \ddots & \vdots & \vdots & \vdots & \ddots & \vdots & \vdots & \ddots & \vdots & \vdots \\
1 & x_\Gamma & \cdots & x_\Gamma^{\,r} & \mathrm{H}_\Gamma & \mathrm{H}_\Gamma x_\Gamma & \cdots & \mathrm{H}_\Gamma x_\Gamma^{\,r} & (1-\mathrm{H}_\Gamma)x_\Gamma^{\,r+1} & \cdots & (1-\mathrm{H}_\Gamma)x_\Gamma^{\,n} & \bullet
\end{bmatrix}$$

$$\begin{bmatrix}
\bullet & (1-\mathrm{H}_0)\eta_0 & \cdots & (1-\mathrm{H}_0)\eta_0 x_0^{\,n} & (1-\mathrm{H}_0)(1+\eta_0)x_0^{\,n+1} & \cdots & (1-\mathrm{H}_0)(1+\eta_0)x_0^{\,m} \\
\vdots & \vdots & \ddots & \vdots & \vdots & \ddots & \vdots \\
\bullet & (1-\mathrm{H}_\gamma)\eta_\gamma & \cdots & (1-\mathrm{H}_\gamma)\eta_\gamma x_\gamma^{\,n} & (1-\mathrm{H}_\gamma)(1+\eta_\gamma)x_\gamma^{\,n+1} & \cdots & (1-\mathrm{H}_\gamma)(1+\eta_\gamma)x_\gamma^{\,m} \\
\vdots & \vdots & \ddots & \vdots & \vdots & \ddots & \vdots \\
\bullet & (1-\mathrm{H}_\Gamma)\eta_\Gamma & \cdots & (1-\mathrm{H}_\Gamma)\eta_\Gamma x_\Gamma^{\,n} & (1-\mathrm{H}_\Gamma)(1+\eta_\Gamma)x_\Gamma^{\,n+1} & \cdots & (1-\mathrm{H}_\Gamma)(1+\eta_\Gamma)x_\Gamma^{\,m}
\end{bmatrix} \tag{52}$$

$$\mathbf{D}=\begin{bmatrix}
p_0+q_0+z_0 \\ p_1+q_1+z_1 \\ \vdots \\ p_r+q_r+z_r \\ z_0-p_0-q_0 \\ z_1-p_1-q_1 \\ \vdots \\ z_r-p_r-q_r \\ p_{r+1}+q_{r+1} \\ \vdots \\ p_n+q_n \\ q_0-p_0 \\ \vdots \\ q_n-p_n \\ q_{n+1} \\ \vdots \\ q_m
\end{bmatrix} \tag{53}$$

The solution can be obtained by solving for **D**, using (47) and substituting the coefficients in (51).

a) Case 2.1: $m>n=r$ (54)

This can be evaluated by substituting the equality $r=n$ in (52) and (53). In (51), all terms of the form $(1-\mathrm{H}_i)(p_j+q_j)x_i^{\,j}$ will be eliminated.

3) Case 3: $m>r>n \;\;\&\;\; r>m>n$ (55)

The overall function is given by:

$$\begin{aligned}
\frac{W}{0.5} &= (p_0+q_0+z_0)+(p_1+q_1+z_1)x+....+(p_n+q_n+z_n)x^n \\
&+\mathrm{H}(z_0-p_0-q_0)+\mathrm{H}(z_1-p_1-q_1)x+...+\mathrm{H}(z_n-p_n-q_n)x^n \\
&+(1-\mathrm{H})*\eta*(q_0-p_0)+.....+(1-\mathrm{H})*\eta*(q_n-p_n)x^n \\
&+(1+\mathrm{H})*z_{n+1}x^{n+1}+.....+(1+\mathrm{H})*z_rx^r \\
&+(1-\mathrm{H})*(1+\eta)*q_{n+1}x^{n+1}+....+(1-\mathrm{H})*(1+\eta)*q_mx^m
\end{aligned} \tag{56}$$

This can be simplified using the matrix notation (43), where:

$$\mathbf{X}=\begin{bmatrix}
1 & x_0 & \cdots & x_0^{\,n} & \mathrm{H}_0 & \mathrm{H}_0x_0 & \cdots & \mathrm{H}_0x_0^{\,n} & (1-\mathrm{H}_0)\eta_0 & \cdots & (1-\mathrm{H}_0)\eta_0x_0^{\,n} & \bullet \\
\vdots & \vdots & \ddots & \vdots & \vdots & \vdots & \ddots & \vdots & \vdots & \ddots & \vdots & \vdots \\
1 & x_\gamma & \cdots & x_\gamma^{\,n} & \mathrm{H}_\gamma & \mathrm{H}_\gamma x_\gamma & \cdots & \mathrm{H}_\gamma x_\gamma^{\,n} & (1-\mathrm{H}_\gamma)\eta_\gamma & \cdots & (1-\mathrm{H}_\gamma)\eta_\gamma x_\gamma^{\,n} & \bullet \\
\vdots & \vdots & \ddots & \vdots & \vdots & \vdots & \ddots & \vdots & \vdots & \ddots & \vdots & \vdots \\
1 & x_\Gamma & \cdots & x_\Gamma^{\,n} & \mathrm{H}_\Gamma & \mathrm{H}_\Gamma x_\Gamma & \cdots & \mathrm{H}_\Gamma x_\Gamma^{\,n} & (1-\mathrm{H}_\Gamma)\eta_\Gamma & \cdots & (1-\mathrm{H}_\Gamma)\eta_\Gamma x_\Gamma^{\,n} & \bullet
\end{bmatrix}$$

$$\begin{bmatrix}
\bullet & (1+\mathrm{H}_0)x_0^{\,n+1} & \cdots & (1+\mathrm{H}_0)x_0^{\,r} & (1-\mathrm{H}_0)(1+\eta_0)x_0^{\,n+1} & \cdots & (1-\mathrm{H}_0)(1+\eta_0)x_0^{\,m} \\
\vdots & \vdots & \ddots & \vdots & \vdots & \ddots & \vdots \\
\bullet & (1+\mathrm{H}_\gamma)x_\gamma^{\,n+1} & \cdots & (1+\mathrm{H}_\gamma)x_\gamma^{\,r} & (1-\mathrm{H}_\gamma)(1+\eta_\gamma)x_\gamma^{\,n+1} & \cdots & (1-\mathrm{H}_\gamma)(1+\eta_\gamma)x_\gamma^{\,m} \\
\vdots & \vdots & \ddots & \vdots & \vdots & \ddots & \vdots \\
\bullet & (1+\mathrm{H}_\Gamma)x_\Gamma^{\,n+1} & \cdots & (1+\mathrm{H}_\Gamma)x_\Gamma^{\,r} & (1-\mathrm{H}_\Gamma)(1+\eta_\Gamma)x_\Gamma^{\,n+1} & \cdots & (1-\mathrm{H}_\Gamma)(1+\eta_\Gamma)x_\Gamma^{\,m}
\end{bmatrix} \tag{57}$$

$$\mathbf{D}=\begin{bmatrix}
p_0+q_0+z_0 \\ p_1+q_1+z_1 \\ \vdots \\ p_n+q_n+z_n \\ z_0-p_0-q_0 \\ z_1-p_1-q_1 \\ \vdots \\ z_n-p_n-q_n \\ q_0-p_0 \\ \vdots \\ q_n-p_n \\ z_{n+1} \\ \vdots \\ z_r \\ q_{n+1} \\ \vdots \\ q_m
\end{bmatrix} \tag{58}$$

The solution can be obtained by using **W** from (44) and solving for **D**, using (47).

a) Case 3.1: $n<m=r$ (59)

This can be evaluated by making a simple substitution $r=m$ in (57) and (58) and evaluating the respective matrices.

4) Case 4: $n>r>m \;\;\&\;\; r>n>m$ (60)

The overall interpolated function takes the following form:

$$\begin{aligned}
\frac{W}{0.5} &= (p_0+q_0+z_0)+(p_1+q_1+z_1)x+....+(p_m+q_m+z_m)x^m \\
&+\mathrm{H}(z_0-p_0-q_0)+\mathrm{H}(z_1-p_1-q_1)x+...+\mathrm{H}(z_m-p_m-q_m)x^m \\
&+(1-\mathrm{H})*\eta*(q_0-p_0)+.....+(1-\mathrm{H})*\eta*(q_m-p_m)x^m \\
&+(1+\mathrm{H})*z_{m+1}x^{m+1}+.....+(1+\mathrm{H})*z_rx^r \\
&+(1-\mathrm{H})*(1-\eta)*p_{m+1}x^{m+1}+....+(1-\mathrm{H})*(1-\eta)*p_nx^n
\end{aligned} \tag{61}$$

The matrices are of the form:

$$\mathbf{X}=\begin{bmatrix} 1 & x_0 & \cdots & x_0^{\,m} & \mathrm{H}_0 & \mathrm{H}_0x_0 & \cdots & \mathrm{H}_0x_0^{\,m} & (1-\mathrm{H}_0)\eta_0 & \cdots & (1-\mathrm{H}_0)\eta_0x_0^{\,m} & \bullet \\ \vdots & \vdots & \ddots & \vdots & \vdots & \vdots & \ddots & \vdots & \vdots & \ddots & \vdots & \vdots \\ 1 & x_\gamma & \cdots & x_\gamma^{\,m} & \mathrm{H}_\gamma & \mathrm{H}_\gamma x_\gamma & \cdots & \mathrm{H}_\gamma x_\gamma^{\,m} & (1-\mathrm{H}_\gamma)\eta_\gamma & \cdots & (1-\mathrm{H}_\gamma)\eta_\gamma x_\gamma^{\,m} & \bullet \\ \vdots & \vdots & \ddots & \vdots & \vdots & \vdots & \ddots & \vdots & \vdots & \ddots & \vdots & \vdots \\ 1 & x_\Gamma & \cdots & x_\Gamma^{\,m} & \mathrm{H}_\Gamma & \mathrm{H}_\Gamma x_\Gamma & \cdots & \mathrm{H}_\Gamma x_\Gamma^{\,m} & (1-\mathrm{H}_\Gamma)\eta_\Gamma & \cdots & (1-\mathrm{H}_\Gamma)\eta_\Gamma x_\Gamma^{\,m} & \bullet \\ \bullet & (1+\mathrm{H}_0)x_0^{\,m+1} & \cdots & (1+\mathrm{H}_0)x_0^{\,r} & (1-\mathrm{H}_0)(1-\eta_0)x_0^{\,m+1} & \cdots & (1-\mathrm{H}_0)(1-\eta_0)x_0^{\,n} & & & & & \\ \vdots & \vdots & \ddots & \vdots & \vdots & \ddots & \vdots & & & & & \\ \bullet & (1+\mathrm{H}_\gamma)x_\gamma^{\,m+1} & \cdots & (1+\mathrm{H}_\gamma)x_\gamma^{\,r} & (1-\mathrm{H}_\gamma)(1-\eta_\gamma)x_\gamma^{\,m+1} & \cdots & (1-\mathrm{H}_\gamma)(1-\eta_\gamma)x_\gamma^{\,n} & & & & & \\ \vdots & \vdots & \ddots & \vdots & \vdots & \ddots & \vdots & & & & & \\ \bullet & (1+\mathrm{H}_\Gamma)x_\Gamma^{\,m+1} & \cdots & (1+\mathrm{H}_\Gamma)x_\Gamma^{\,r} & (1-\mathrm{H}_\Gamma)(1-\eta_\Gamma)x_\Gamma^{\,m+1} & \cdots & (1-\mathrm{H}_\Gamma)(1-\eta_\Gamma)x_\Gamma^{\,n} & & & & & \end{bmatrix} \tag{62}$$

$$\mathbf{D}=\begin{bmatrix} p_0+q_0+z_0 \\ p_1+q_1+z_1 \\ \vdots \\ p_m+q_m+z_m \\ z_0-p_0-q_0 \\ z_1-p_1-q_1 \\ \vdots \\ z_m-p_m-q_m \\ q_0-p_0 \\ \vdots \\ q_m-p_m \\ z_{m+1} \\ \vdots \\ z_r \\ p_{m+1} \\ \vdots \\ p_n \end{bmatrix} \tag{63}$$

The coefficients of **D** are solved using (47) and are used to generate the overall interpolated function **W**.

a) Case 4.1: $m=n<r$ (64)

This can be evaluated by substituting the equality $n=m$ in (62) and (63). In (61), all terms of the form $(1-\mathrm{H}_i)*(1-\eta_i)*p_j x_i^{\,j}$ will be eliminated.

b) Case 4.2: $m<n=r$ (65)

This can be evaluated by substituting the equality $r=n$ in (62) and (63).

5) Case 5: $m=n=r$ (66)

This is the simplest and most basic case. This condition can be easily evaluated by substituting $r=m=n$ in **X** and **D**. In the expression for the overall function, W simplifies to:

$$\begin{aligned} \frac{W}{0.5} &= (p_0+q_0+z_0)+(p_1+q_1+z_1)x+....+(p_n+q_n+z_n)x^n \\ &+\mathrm{H}(z_0-p_0-q_0)+\mathrm{H}(z_1-p_1-q_1)x+...+\mathrm{H}(z_n-p_n-q_n)x^n \\ &+(1-\mathrm{H})*\eta*(q_0-p_0)+.....+(1-\mathrm{H})*\eta*(q_n-p_n)x^n \end{aligned} \tag{67}$$

The substitution $m=n=r$ can be made in **X** and **D** of any of the above cases and sub-cases discussed. All terms of the following form $(1-\mathrm{H}_i)(p_j+q_j)x_i^j$, $(1+\mathrm{H}_i)*z_j*x_i^j$, $(1-\mathrm{H}_i)*(1+\eta_i)*q_j*x_i^j$ and $(1-\mathrm{H}_i)*(1-\eta_i)*p_j*x_i^j$ will be eliminated.

C. Multi-region Hyperbolic Tangent Interpolation

Let us generalize the above discussed interpolation technique. Let there be α regions defined, with each region being spanned by a polynomial S_R, where R stands for each individual region. The hyperbolic tangent functions will also be uniquely defined for each independent region. The number of TANH functions will be one lesser than the number of polynomials.

$$S_R(x)\rightarrow S_1,S_2,.....,S_{\alpha-1},S_\alpha$$

and

$$\eta_R(x)\rightarrow \eta_1,\eta_2,.....,\eta_{\alpha-1}$$

The overall generalized interpolated function $I(x)$, over α regions takes the following form:

$$\begin{aligned} \frac{I}{0.5} &= (S_1+S_2+.....+S_\alpha)+\eta_{\alpha-1}*(S_\alpha-S_{\alpha-1}-.....-S_1) \\ &+(1-\eta_{\alpha-1})*\eta_{\alpha-2}*(S_{\alpha-1}-S_{\alpha-2}-.....-S_1) \\ &+(1-\eta_{\alpha-1})*(1-\eta_{\alpha-2})*\eta_{\alpha-3}*(S_{\alpha-2}-S_{\alpha-3}-.....-S_1) \\ &+(1-\eta_{\alpha-1})*(1-\eta_{\alpha-2})*(1-\eta_{\alpha-3})*\eta_{\alpha-4}*(S_{\alpha-3}-.....-S_1) \\ &+.....+(1-\eta_{\alpha-1})*(1-\eta_{\alpha-2})*....*\eta_1*(S_2-S_1) \end{aligned} \tag{68}$$

III. Application of the TANH Interpolation Technique to BK Ion Channel Modelling

The BK ion channel is being modelled for the detrusor smooth muscle tissue. This channel could be modelled if it were possible to quantify its dependence on voltage and intracellular calcium concentration. However, the experimental data providing this dependence are quite sparse.

Various kinetic models have been built for this channel using Markov process modelling. The kinetic states were decided by the number of calcium ions binding to the channel protein [13, 14]. These models are regarded as some of the best prototypes existing for calcium activated channels, in general.

Amongst smooth muscles, BK channel has been developed for uterine smooth muscles [15]. It was noted that the experimental results, exclusively for this channel, were drawn from two different papers [16, 17]. However, unlike [15], experimental data for the detrusor smooth muscle tissue was quite sparse.

In this work, we have tried to model this BK channel for detrusor smooth muscle using the Hodgkin-Huxley technique.

The BK channel current is expressed as:

$$I_{BK}=g_{\max}*m^4*(ah^4+(1-a))*(v-E_K) \tag{69}$$

where

I_{BK} – BK channel currents

$g_{\max}$ – Maximum conductance expressed by the BK channels in the cell

v – Membrane voltage / potential

E_K – Nernst potential of potassium ion $= -85mV$

m – Activation parameter

h – Inactivation parameter

a – Modulates the extent of inactivation

$a = 0 \Rightarrow$ No Inactivation

$a = 1 \Rightarrow$ Complete Inactivation

Here,

$$m = m_\infty - (m_\infty - m_0)\, e^{-t/\tau_m} \tag{70}$$

$$h = h_\infty - (h_\infty - h_0)\, e^{-t/\tau_h} \tag{71}$$

The activation parameter of the BK channel is strongly dependent on both membrane depolarization as well as the intracellular calcium concentration. Figure 6A from Zakharov *et al.* [18] depicted a plot of the activation parameter with respect to membrane depolarization, for different values of the intracellular calcium concentration.

We generated the exact same sigmoidal trends reported in Figure 6A of Zakharov *et al.* [18] by using the Boltzmann equation of the form reported in (72). These curves that we fitted are depicted in Figure 4.

$$m_\infty \triangleq \frac{g}{g_{\max}} = 0.05 + \frac{0.95}{1 + e^{-\left[\frac{(v - V_{0.5}(\zeta))}{\sigma(\zeta)}\right]}} \tag{72}$$

where,

ζ – Intracellular calcium concentration

g – Channels' conductance at a particular 'v'

$V_{0.5}$ – Half-activation voltage

σ – Slope factor

The half-activation voltage signifies the potential at which the channels are half-maximally activated. The slope factor, as the name suggests, graphically describes the steepness of rise of the activation curve.

The trends were similar and what changed between each calcium concentration were $V_{0.5}$ and σ. The computationally fitted graphs are shown in Figure 4 and the values of $V_{0.5}$ and σ are tabulated with respect to different calcium concentrations (Table I).

Since the experiment was carried out for four intracellular calcium concentrations, only four values of $V_{0.5}$ and σ were available to predict its trend. The plot of $V_{0.5}$ vs ζ had an exponentially decreasing trend and fitting that was relatively simple.

In the case of the slope factor, the trend was not monotonic and it was necessary to capture this multi-phasic trend. Since the data points were minimal, none were omitted under the assumption of an "experimental error" or "outlier". We decided to interpolate the given set of data points with the two-region TANH spline function.

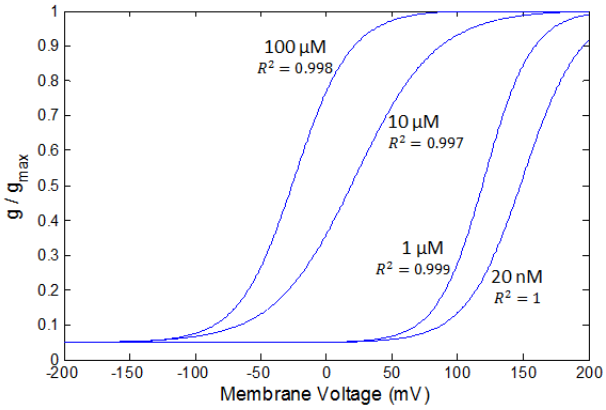

Figure 4. Activation parameter of BK channels vs membrane potential, for different intracellular calcium concentrations. The blue solid lines have been generated using the Boltzmann equation of the form reported in (72). The fit with respect to the reported experimental data taken from Figure 6A of Zakharov *et al.* [18] is indicated through the R^2 value at each intracellular calcium concentration.

TABLE I.

ζ (µM)	$V_{0.5}$ (mV)	σ (mV)
100	-24.056	21.2
10	22.12	30.5
1	120.67	17.9
0.02	150.00	21.5

A. *Implementing Two-region TANH Spline function on Sparse data*

The bottom three values of Table I, i.e., the ones corresponding to 20 nM, 1 µM and 10 µM were grouped together to form $P_n(\zeta)$ whereas the fourth point, 100 µM, was $Q_m(\zeta)$. The data set was divided into two regions, one over which $P_n(\zeta)$ was valid, and the other over which $Q_m(\zeta)$ was valid. These two regions were then braided together using the TANH spline interpolation technique. The transition point was chosen to be $\xi_n = 10\mu M$ and the rate of transition as $k = 1$.

The overall expression for slope factor was of the form:

$$\sigma = 0.5*[(p_0 + q_0) + \eta(q_0 - p_0) + (1-\eta)\, p_1\zeta + (1-\eta)\, p_2\zeta^2] \tag{73}$$

Using (18) and (25), we can solve for **B**. The values of η, ζ and σ are tabulated in Table II. On solving we obtain:

$$\frac{\mathbf{B}}{2} = \begin{bmatrix} 0.5*(p_0 + q_0) \\ 0.5*(q_0 - p_0) \\ 0.5*p_1 \\ 0.5*p_2 \end{bmatrix} = \begin{bmatrix} 21.39285 \\ -0.19285 \\ -2.14881 \\ 0.305952 \end{bmatrix} \tag{74}$$

TABLE II.

$k=1$ $\gamma=3$ $n=2$ $m=0$ $\xi_n=10\mu M$		
η = tanh(ζ – ξₙ)	**ζ (μM)**	**σ (mV)**
-1	0.02	21.5
-1	1	17.9
0	10	30.5
1	100	21.2

TABLE III.

$\xi=10\mu M$ $k=0.1$					
SN	**ζ μM**	**f (ζ)**	**P (ζ)**	**Q(ζ) * g(ζ)**	**σ (mV) = P(ζ) f(ζ) + Q(ζ) g(ζ)**
1	0.02	0.880	20.301	2.536	20.408
2	0.1	0.879	19.772	2.572	19.945
3	0.25	0.875	18.806	2.641	19.104
4	0.5	0.870	17.274	2.758	17.785
5	0.75	0.864	15.839	2.881	16.567
6	1	0.858	14.500	3.007	15.450
7	10	0.500	30.508	10.60	25.854
8	100	0.000	7062.96	21.20	21.200

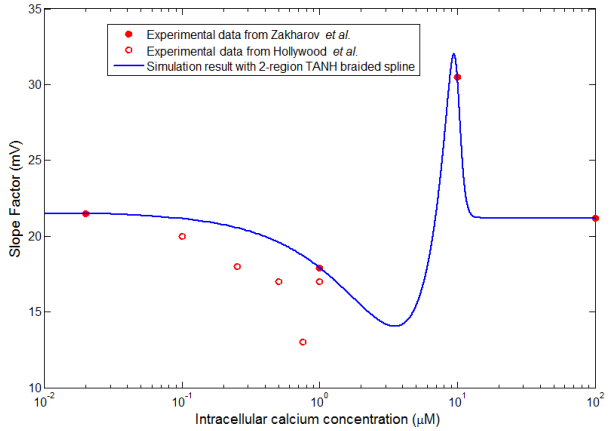

Figure. 5. The curve fit obtained for the slope factor data (red filled circles) taken from Figure 6A of Zakharov *et al.* [18] after interpolating with two-region TANH spline (blue solid line). The graph also plots the additional experimental slope factor data that was procured from Hollywood *et al.* [19] (red unfilled circles).

The overall equation of the slope factor is as follows:

$$\sigma = 21.39285 - 0.19285\eta - (2.14881*(1-\eta)*\zeta) + (0.305952*(1-\eta)*\zeta^2) \quad (75)$$

Given the existing sparse range of data, the interpolated function is shown in Figure 5. The values taken up by the slope factor fall within physiological ranges. Also, the overall function is finite, continuous and differentiable.

B. Effectiveness of the Two-region TANH Spline interpolation technique

In another study by Hollywood *et al.* [19], the effect of intracellular calcium on BK channels in sheep urethra smooth muscle cells were investigated. The half-activation voltages and the slope factors were tabulated in Table 1 of Hollywood *et al.* [19]. Here, the intracellular calcium concentrations were varied over a very narrow range i.e., they were between 0.1 μM and 1 μM.

These additional data points have been plotted in Figure 5, (red unfilled circles). It can be observed that these additional data follow the same trend as predicted by (75) (blue solid line). This finding was crucial since it enforces the fact that the TANH braided spline not only interpolates sparse data but can also accurately predict the actual underlying trend.

There exists a cluster of closely spaced data points for only a very narrow range of intracellular calcium concentration ($0.1\mu M - 1\mu M$). Despite extensive search, no similar published experimental data was found for higher intracellular calcium concentrations.

Hence, the data procured from Table 1 of Hollywood *et al.* [19] were combined with the existing set (shown in Table I of this paper). The data in Table I (of this paper) could not be ignored because it documented the channel's behavior at higher calcium concentrations ($\geq 1\mu M$).

Since there exists ample data for lower calcium concentrations, we decided to test the effectiveness of the TANH spline interpolation technique, by approximating this ample data. This approximation was carried out by performing a least-squares fit. However, the data continued to remain sparse in the higher range of calcium concentration. Thus, the two-region TANH spline function was used to braid the sparse data present at the higher calcium concentration, with the function approximating the abundant data present at the lower calcium concentration.

The TANH spline functions chosen had $\xi=10\mu M$ and $k=0.1$:

$$f(\zeta) = 0.5 - (0.5*\tanh(k*(\zeta-\xi))) \quad (76)$$

$$g(\zeta) = 0.5 + (0.5*\tanh(k*(\zeta-\xi))) \quad (77)$$

$$Q(\zeta) = 21.2 \quad (78)$$

However, $P(\zeta)$ was obtained by performing a least-squares fit on the remaining points (i.e., 1-2-3-4-5-6-7 from Table III).

$$P(\zeta) = 20.43448 - 6.70571\zeta + 0.77131\zeta^2 \quad (79)$$

The calculations have been tabulated in Table III. The slope factor is given by (80) and is plotted in Figure 6.

$$\sigma = P(\zeta)*f(\zeta) + Q(\zeta)*g(\zeta) \quad (80)$$

Figure 6 was generated using approximation while Figure 5 was generated using interpolation. Despite the differences in approach, it must be noted that the two plots are quite similar. Thus, TANH spline interpolation helped predicting the right trend despite the presence of sparse data, thereby making it a highly robust technique.

C. Implementing the Three-region TANH Spline function

Sometimes, the data distribution is such that dividing them into two regions and interpolating them may not yield a suitable trend, or the function may assume values that are physiologically inadmissible. The data though abundant,

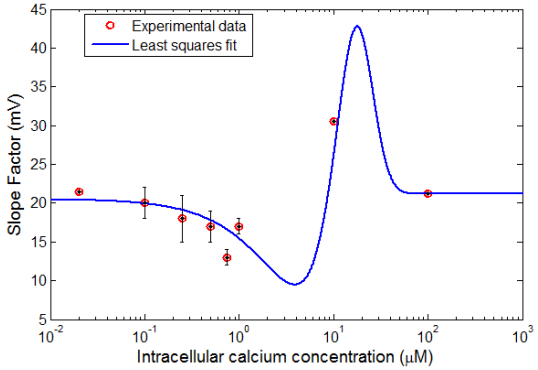

Figure 6. The curve is generated by performing a least-squares fit on the first seven data points, which is then interpolated with the eighth data point using the two-region TANH spline function. The black vertical bars indicate the range of values that the slope factor can assume at that concentration, as documented in Table 1 of Hollywood *et al.* [19]. The other data points, without the error bars, were obtained from Zakharov *et al.* [18].

might be scattered in a way that the user loses control over the interpolated function by restricting the distribution to two regions. To exercise more control over the values attained by the function, we need to employ a slightly modified technique.

Even though it has been demonstrated that the current data set can be easily interpolated with two-region TANH braided spline, we are considering the same set of data to implement three-region TANH interpolation technique, as a proof of concept.

The first region was constructed by grouping 20 nM, 0.1 µM and 0.25 µM. The second region was constructed with 0.75 µM and 10 µM. The third region comprised solely of 100 µM.

The expression for slope factor has the following form:

$$\frac{\sigma}{0.5} = (p_0 + q_0 + z_0) + \mathrm{H}(z_0 - p_0 - q_0) + (1-\mathrm{H})(p_1 + q_1)\zeta$$
$$+(1-\mathrm{H})*\eta*(q_0 - p_0) + (1-\mathrm{H})*\eta*(q_1 - p_1)\zeta \qquad (81)$$
$$+(1-\mathrm{H})*(1-\eta)*p_2\zeta^2$$

The calculations have been tabulated in Table IV. **D** can be evaluated using (44), (45) and (47).

$$\frac{\mathbf{D}}{2} = \begin{bmatrix} 18.4319 \\ 2.768092 \\ -5.17015 \\ -3.39611 \\ 6.716573 \\ 15.75311 \end{bmatrix} \qquad (82)$$

The final interpolated expression for slope factor is provided in (83) and the plot is indicated with blue solid lines in Figure 7.

$$\sigma = 18.4319 + (2.768092*\mathrm{H}) - (5.17015*(1-\mathrm{H})*\zeta)$$
$$-(3.39611*(1-\mathrm{H})*\eta) + (6.716573*(1-\mathrm{H})*\eta*\zeta) \qquad (83)$$
$$+(15.75311*(1-\mathrm{H})*(1-\eta)*\zeta^2)$$

TABLE IV.

	$k=5$	$\xi = 0.35\mu M$	$K=0.1$	$\Xi = 10\mu M$
SN	**ζ (µM)**	**η = tanh(k*(ζ - ξ))**	**H = tanh(K*(ζ - Ξ))**	**σ (mV)**
1	0.02	-0.9288576	-0.7607529	21.5
2	0.1	-0.8482836	-0.7573623	20
3	0.25	-0.4621172	-0.7508933	18
5	0.75	0.9640276	-0.7282542	13
7	10	1	0	30.5
8	100	1	1	21.2

TABLE V.

	$k=5$	$\xi = 0.35\mu M$	$K=0.1$	$\Xi = 10\mu M$
SN	**ζ (µM)**	**η = tanh(k*(ζ - ξ))**	**H = tanh(K*(ζ - Ξ))**	**σ (mV)**
1	0.02	-0.92886	-0.76075	21.5
2	0.1	-0.84828	-0.75736	20
3	0.25	-0.46212	-0.75089	18
4	0.5	0.635149	-0.73978	17
6	1	0.996998	-0.7163	17
7	10	1	0	30.5
8	100	1	1	21.2

The same data set could also be divided in a different manner. The first region could be constructed by grouping 20 nM, 0.1 µM, 0.25 µM and 0.5 µM; the second with 1 µM and 10 µM and the third region with 100 µM.

Using the exact same approach, the expression for slope factor was found (84) and is plotted in broken blue lines in Figure 7. The calculations have been tabulated in Table V.

$$\sigma = 19.5597 + (1.640299*\mathrm{H}) - (4.61883*(1-\mathrm{H})*\zeta)$$
$$-(2.16463*(1-\mathrm{H})*\eta) + (5.929322*(1-\mathrm{H})*\eta*\zeta) \qquad (84)$$
$$+(3.006487*(1-\mathrm{H})*(1-\eta)*\zeta^2)$$
$$+(16.51641*(1-\mathrm{H})*(1-\eta)*\zeta^3)$$

Figure 7 depicts the trend of slope factor with respect to variations in intracellular calcium concentrations by employing the three-region TANH braided spline interpolation. If we compare Figure 5 and Figure 7, we can observe that the trends followed by the slope factor, in both cases, are quite similar. Along with this, the functions attain values that are physiologically tenable.

A few interesting observations can be made from Figure 7. The slope factor seems to be steady at around 21 mV at intracellular calcium concentrations $\leq 0.02\mu M$ and $\geq 100\mu M$. It is in the concentration range in between these limits where the slope factor varies in a seemingly characteristic pattern.

It must be noted that both (83) and (84) seem to be equally likely to govern the trend of slope factor. If there had been more data available, the exact trend could have

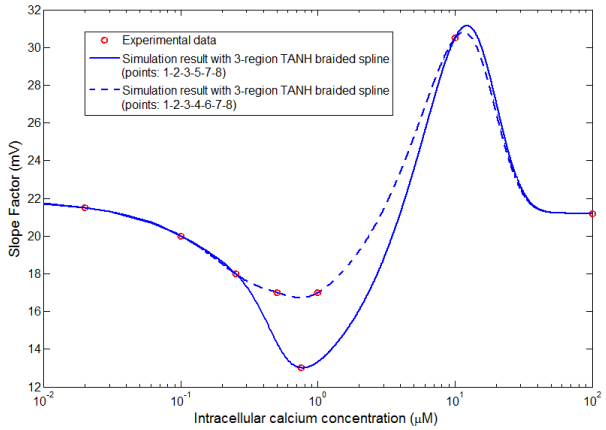

Figure 7. The curve fit obtained for the slope factor after interpolating the data with three-region TANH braided spline function.

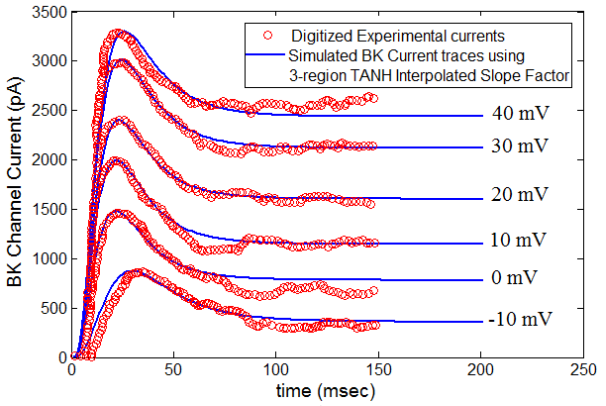

Figure 8. BK channel current output for detrusor smooth muscles. The blue solid lines indicate simulated BK channel currents obtained by employing three-region TANH interpolated slope factor (83) in the activation parameter. Red circles indicate the published experimental BK channel currents that have been manually digitized from Figure 1Ba in Hirano *et al.* [22].

been ascertained. However, given the current set of data, we can simply propose the possible trends that the slope factor can assume. For instance, it appears as if (83) and (84) seem to mark the extreme limits of this parameter's trend.

However, apart from these discernable features, we could test the implementation of this three-region slope factor in generating BK channel currents.

D. BK Channel Model

The BK channel was modelled along the lines of Hodgkin-Huxley model for potassium ion channels, as stated in (69), (70) and (71) of Section III. The remaining model parameters, namely h_∞, time constant of activation (τ_m) and time constant of inactivation (τ_h) were obtained from prior work [3, 20, 21 and 22]. The model for BK channel was thus created. With the slope factor in place, m_∞ (72) was complete.

An attempt was made to generate the BK currents depicted in Figure 1Ba from Hirano *et al.* [22]. These currents were recorded from the guinea-pig urinary bladder smooth muscle cells.

It has already been illustrated in Figure 4 from Gupta *et al.* [1], that the implementation of two-region slope factor will successfully replicate the experimental BK channel currents. We also tested the slope factor obtained by least-squares fit (80) and found that it generated similar current profiles (not shown). However, the three-region slope factor needed to be tested in the existing BK model.

The BK channel currents were simulated by employing the slope factor, expressed in both (83) and (84), in the activation parameter. Both these equations generated the same current profiles. For simplicity, we have shown the currents obtained by incorporating (83) as the slope factor (Figure 8).

The activation characteristics as well as the overall trend of the currents are very close to the ones reported in Figure 1Ba of Hirano *et al.* [22]. Thus, by implementing multi-region interpolation technique, the simulated BK channel currents faithfully replicated the experimentally recorded channel currents.

One could choose either two-region or multi-region interpolation technique based on the number of data points available, its distribution as well as the control that the user might need to exercise on the values assumed by the interpolating function. Hence, this technique can be suitably adapted to any scenario.

IV. Discussion

Channels play an integral role in conveying electrical signals within the body. These are integral protein structures that are found on the surface of the cell membrane. These allow passage of ions between the intracellular fluid and the extracellular fluid. There are many different ion channels present in the body and each of these has its own specific dynamics. In order to understand how a channel behaves, it is necessary to capture these dynamics.

Large variations in channel density and molecular complexity coupled with the lack of selective blockers constrain the extent to which one can experiment on a channel. In many cases, the resources available allow one to gain insights into the channel behavior and functioning. However, these may not be sufficient to decode all the different aspects, such as the interdependencies of the channel's gating parameters. Typically, channels are studied with the help of pharmacology, electrophysiology and molecular characterization. Even in these studies, it is quite challenging to test various aspects of the channel's properties. Even while testing channel parameters, care is to be taken to ensure that the cell is not damaged. Hence, in order to computationally model a channel's dynamics, one has to rely on electrophysiological recordings [22], functional [6] and pharmacological studies [23].

When modelling ion channels, it is necessary to accurately mimic experimentally recorded currents. In order to do this, it is critical to develop equations that precisely capture the dependency of model parameters on key physiological variables. In this work, these variables are membrane potential and intracellular calcium concentration.

In the case of parameters for which data are sparse, or abundant but scattered, conventional techniques run the danger of neglecting some of the data points. While omitting data points, one runs the risk of eliminating inherent crucial information about channel properties that might be hidden within the "outlier" nature of the data point.

When data points for the parameters of interest are abundant and well distributed, curve fitting can furnish empirical equations for its dependencies, as has been done in [15]. However when data is sparse, such approaches can result in significant errors in the formulation of the defining equations. Similarly, if there exists abundant data but without a perceptible underlying trend, forming equations will be challenging. With the technique reported here, sparse data as well as sufficient yet scattered data will not be a constraint for its use in modelling. Moreover, it serves to capture all available data points more inclusively, as well as predict the underlying trend accurately, thus offering important advantages in such situations.

Here, the focus has been on generating an analytical function for the slope factor, which has been incorporated in the activation parameter of BK channel. The parameter data as well as the BK channel currents were specific to smooth muscles.

The TANH technique was proposed to be an interpolation technique that can be employed when data are sparse [1]. However, these techniques do not actually serve any purpose if the actual physiological trend differs from the one predicted. When additional data was procured from Hollywood *et al.* [19], it was found that the trend that was predicted by the TANH interpolation technique resembled the trend that was obtained experimentally in [19]. This was further verified by performing a least-squares fit on the additional data. Thus, TANH braided spline can be used in numerous applications.

This technique can be applied more generally to other tissues and other ion channels as well. For example, Figures 2D, 2E, and 2G in Herzog *et al.* [12] have documented experimental and simulated activation and inactivation time constants for TTX-sensitive and TTX-resistant sodium channels in spinal sensory neurons. Their model curves show a certain degree of fit with the experimental curves. However, by implementing the TANH braided spline, the resulting functions can provide a better fit. One might opt to choose a two-region interpolation, where the rising and falling edges of the time constants could be approximated by separate functions, which can then be braided to provide the overall function. This has already been illustrated in Figure 2 in Section II A. The black dotted lines in the figure illustrates the function that the authors of Herzog *et al.* [12] had chosen to approximate their experimental data points (red circles) in Figure 2E Herzog *et al.* [12]. The blue solid line is the function obtained through TANH interpolation, as detailed in Section II A.

Similarly, Figure 2D in Scholz *et al.* [24] can be used as an example of how this technique could be implemented for sparse data. This figure plots the open probability of calcium activated potassium channels verses the (common logarithm of) intracellular calcium concentration. This was plotted for four different membrane potentials and each plot had three-four calcium concentration data points. These data points were linearly interpolated for the purpose of depiction. We could use TANH braided spline in order to create an empirical function correlating the open probability with intracellular calcium concentration.

V. Conclusion

The TANH braided spline results in a single function over the whole range, continuous and differentiable to any arbitrary order. It also additionally has the property that the model can be made to settle to a "steady state" outside the region under consideration. In situations where model equations have inter-dependencies, a single computationally compact function has the added advantage of being easier to implement inside a simulator.

We have implemented the TANH spline interpolation technique for a certain parameter, slope factor, of the BK channel in smooth muscle. We had earlier described the utility of this technique in cases where parameters were characterized by sparse data [1]. In the work reported here, we reveal the robustness of this technique in its ability to accurately predict the underlying trend, despite sparse data.

Along with this, we also introduce and demonstrate the employability of the multi-region TANH spline interpolation technique. This technique could be implemented if the user has abundant data points scattered over a wide range, in a way such that its underlying trend remains elusive. Based on the number of data points, as well as its range, the user can determine the number of regions and hence, incorporate a suitable multi-region TANH spline function. Multi-region TANH spline function further equips the user to restrict the values assumed by the interpolating function at intermediate data points.

Both these techniques resulted in functions that were equally mathematically consistent and physiologically viable. Both yielded simulated BK channel currents that mimicked the experimentally recorded ones.

Thus, one can consequently visualize this technique as one that allows direct use of experimental data for behavioral evaluation in a computational environment such as a simulator.

References

[1] S. Gupta and R. Manchanda, "TANH Spline Interpolation for Analytical Modelling of BK Ion Channels in Smooth Muscle", in *2014 8th Asia Modelling Symposium; International Conference on Mathematical Modelling and Computer Simulation*, Taipei & Kuala Lumpur, pp. 71–76, Sep. 2014.

[2] G. Petkov, "Role of potassium ion channels in detrusor smooth muscle function and dysfunction", *Nature Reviews Urology*, vol. 9, no. 1, pp. 30–40, Jan. 2012.

[3] G. Herrera, T. Heppner and M. Nelson, "Voltage dependence of the coupling of Ca^{2+} sparks to BK_{Ca} channels in urinary bladder smooth muscle", *American Journal of Physiology – Cell Physiology*, vol. 280, no. 3, pp. C481–C490, Mar. 2001.

[4] T. Heppner, A. Bonev and M. Nelson, "Ca(2+)–activated K+ channels regulate action potential repolarization in urinary bladder smooth muscle", *American Journal of Physiology – Cell Physiology*, vol. 273, no. 1, pp. C110–C117, Jul. 1997.

[5] G. Petkov, "Central role of the BK channel in urinary bladder smooth muscle physiology and pathophysiology", *American Journal of Physiology – Regulatory, Integrative and Comparative Physiology*, vol. 307, no. 6, pp. R571–R584, Sep. 2014.

[6] B. Darblade *et al.*, "Effects of potassium channel modulators on human detrusor smooth muscle myogenic phasic contractile activity: Potential therapeutic targets for overactive bladder", *Urology*, vol. 68, iss. 2, pp. 442–448, Aug. 2006.

[7] A. Meredith, K. Thorneloe, M. Werner, M. Nelson and R. Aldrich, "Overactive Bladder and Incontinence in the Absence of the BK Large Conductance Ca^{2+}–activated K^+ Channel", *The Journal of Biological Chemistry*, vol. 279, no. 35, iss. 27, pp. 36746–36752, Jun. 2004.

[8] K. Hristov, S. Afeli, S. Parajuli, Q. Cheng, E. Rovner and G. Petkov, "Neurogenic Detrusor Overactivity Is Associated with Decreased Expression and Function of the Large Conductance Voltage–and Ca^{2+}–Activated K^+ Channels", *PLoS ONE*, vol. 8, no. 7: e68052, pp. 1–8, Jul. 2013.

[9] G. Herrera and M. Nelson, "Differential regulation of SK and BK channels by Ca^{2+} signals from Ca^{2+} channels and ryanodine receptors in guinea-pig urinary bladder myocytes", *The Journal of Physiology*, vol. 541, iss. 2, pp. 483–492, Jun. 2002.

[10] Spline (mathematics). (n.d.). *Wikipedia*.
Available: http://en.wikipedia.org/wiki/Spline_(mathematics). Accessed May. 27, 2014.

[11] S. Liu. "Spline Interpolation".
Available: http://www.geos.ed.ac.uk/~yliu23/docs/lect_spline.pdf. Accessed May. 27, 2014.

[12] R. Herzog, T. Cummins and S. Waxman, "Persistent TTX–Resistant Na^+ Current Affects Resting Potential and Response to Depolarization in Simulated Spinal Sensory Neurons", *Journal of Neurophysiology*, vol. 86, no. 3, pp. 1351–1364, Sep. 2001.

[13] E. Moczydlowski and R. Latorre, "Gating Kinetics of Ca^{2+}– activated K^+ Channels from Rat Muscle Incorporated into Planar Lipid Bilayers: Evidence for two voltage–dependent Ca^{2+} binding reactions", *The Journal of General Physiology*, vol. 82, no. 4, pp. 511–542, Oct. 1983.

[14] L. Shao, R. Halvorsrud, L. Borg-Graham and J. Storm, "The role of BK–type Ca^{2+}–dependent K^+ channels in spike broadening during repetitive firing in rat hippocampal pyramidal cells", *The Journal of Physiology*, vol. 521, iss. 1, pp. 135–146, Nov. 1999.

[15] W. Tong, C. Choi, S. Karche, A. Holden, H. Zhang and M. Taggart, "A Computational Model of the Ionic Currents, Ca^{2+} Dynamics and Action Potentials Underlying Contraction of Isolated Uterine Smooth Muscle", *PLoS ONE*, vol. 6, no. 4: e18685, pp. 1–21, Apr. 2011.

[16] L. Bao and D. Cox, "Gating and Ionic Currents Reveal How the BK_{Ca} Channel's Ca^{2+} Sensitivity Is Enhanced by its β1 Subunit", *The Journal of General Physiology*, vol. 126, no. 4, pp. 393–412, Sep. 2005.

[17] P. Orio *et al.*, "Structural Determinants for Functional Coupling Between the β and α Subunits in the Ca^{2+}–activated K^+ (BK) Channel", *The Journal of General Physiology*, vol. 127, no. 2, pp. 191–204, Jan. 2006.

[18] S. Zakharov, J. Morrow, G. Liu, L. Yang and S. Marx, "Activation of the BK (SLO1) Potassium Channel by Mallotoxin", *The Journal of Biological Chemistry*, vol. 280, no. 35, iss. 2, pp. 30882–30887, Jul. 2005.

[19] M. Hollywood, K. McCloskey, N. McHale and K. Thornbury, "Characterization of outward K^+ currents in isolated smooth muscle cells from sheep urethra", *American Journal of Physiology – Cell Physiology*, vol. 279, no. 2, pp. C420–C428, Aug. 2000.

[20] P. Lovell, D. James and D. McCobb, "Bovine Versus Rat Adrenal Chromaffin Cells: Big Differences in BK Potassium Channel Properties", *Journal of Neurophysiology*, vol. 83, no. 6, pp. 3277–3286, Jun. 2000.

[21] X. Xia, J. Ding and C. Lingle, "Molecular Basis for the Inactivation of Ca^{2+}–and Voltage–Dependent BK Channels in Adrenal Chromaffin Cells and Rat Insulinoma Tumor Cells", *The Journal of Neuroscience*, vol. 19, no. 13, pp. 5255–5264, Jul. 1999.

[22] M. Hirano, Y. Imaizumi, K. Muraki, A. Yamada and M. Watanabe, "Effects of ruthenium red on membrane ionic currents in urinary bladder smooth muscle cells of the guinea-pig", *Pflügers Archiv–European Journal of Physiology*, vol. 435, iss. 5, pp. 645–653, Mar. 1998.

[23] G. Kaczorowski and M. Garcia, "Pharmacology of voltage–gated and calcium–activated potassium channels", *Current Opinion in Chemical Biology*, vol. 3, iss. 4, pp. 448–458, Aug. 1999.

[24] A. Scholz, M. Gruß and W. Vogel, "Properties and functions of calcium–activated K^+ channels in small neurones of rat dorsal root ganglion studied in a thin slice preparation", *The Journal of Physiology*, vol. 513, iss. 1, pp. 55–69, Nov. 1998.